Fizika Nizkikh Temperatur, 2001, v. 27, No. 1, p. 90–95

Relaxation dynamics in the high-frequency crystal-field spectroscopy of $PrNi_5$ point contacts

O. P. Balkashin[1,2], T. M. Brill[2], A. G. M. Jansen[2], G. L. Sukhodub[1], P. Wyder[2], and I. K. Yanson[1]

[1] *B. Verkin Institute for Low Temperature Physics and Engineering, National Academy of Science of Ukraine, 47 Lenin Ave., 310164 Kharkov, Ukraine*

[2] *Grenoble High Magnetic Field Laboratory, Max-Planck-Institute für Festkörperforschung and Centre National de la Recherche Scientifique, B.P. 166, F-38042 Grenoble Cedex 09, France*
E-mail: balkashin@ilt.kharkov.ua

Received July 7, 2000

High-frequency point-contact (PC) spectroscopy is used to investigate the relaxation processes kinetics in the intermetallic rare-earth compound $PrNi_5$. A difference is observed in the spectral response between the conventional low-frequency PC data and the response signal to microwave and far-infrared radiation of $PrNi_5$–Cu point contacts. This difference is connected with the f-shell electronic levels (CEF levels) and phonon temporal dynamics. The phonon reabsorption contribution to the spectra above the Debye energy *decreases* for microwave and far-infrared frequencies. However, the crystal-field contribution to the spectra at 4.2 meV is *enhanced* for high frequencies reflecting the relaxation processes specific for these Fermi-statistics electron excitations. The characteristic frequency for CEF-level relaxation is evaluated as ~ 200 GHz.

PACS: **72.30.+q**, 73.40.Jn

Introduction

The crystal-electric-field (CEF) level excitations determine the magnetic, thermodynamic, and transport properties of the intermetallic rare-earth compound $PrNi_5$ [1,2]. The temperature dependences of these characteristics show a Schottky-like anomaly at $T \sim 15$ K. It arises from the ground state splitting of the $4f$ electrons of the Pr^{3+} ions in the CEF of hexagonal symmetry. A crystal-field eigenstate scheme of $PrNi_5$ has been estimated both from neutron diffraction experiments [3] and point-contact-spectroscopy measurements [4,5].

Point-contact spectroscopy is dealing with the nonlinear correction to the current-voltage (I-V) characteristics of a PC. This method has been successfully employed for estimating the energy relaxation spectra of quasiparticle excitations in many metals and compounds under steady-state conditions [6–8]. Recently, high-frequency PC spectroscopy has been developed and applied to investigating the relaxation kinetics of the electron-phonon system and the temperature in metallic contacts [9–11]. The PC spectra measurements over a wide frequency range make it possible to separate different transient phenomena in PCs and evaluate the appropriate relaxation times.

In accordance with the theory [12] the second-order derivative of the I-V curve (PC spectrum) for a contact formed by rare-earth metals with two-level splitting Δ of the f-shell states consists of three nonlinear contributions to the conductivity* :

$$-\frac{d^2I}{dV^2}(eV) \sim g_f(eV) + \left[\frac{1}{2}\, g_f(eV) - 4\Delta^2 \int_0^{eV} \frac{g_f(\varepsilon)}{(\varepsilon + eV)^3}\, d\varepsilon\right], \qquad (1)$$

where the first term $g_f(eV)$, the PC spectral function of the CEF-level excitations, is due to inelastic f-shell excitations by conduction electrons. The

* The small term connected with elastic scattering processes is neglected in Eq. (1).

other term, in brackets, describes the background signal and is determined by two different mechanisms. The first one is the reverse CEF-excitation transitions from the excited to the ground state, which enhance the direct transitions probability. The second is the increasing of the excited-state population and the decreasing of the ground-state population with voltage gain that decreases the probability of the inelastic scattering processes.

It should be noted that the CEF-level spectral function $g_f(eV)$ depends on the CEF-level population because of the Fermi statistics of the excitations [12],

$$g_f(eV) = N(0)n_f(N_k - N_i) << |W^{ik}_{\mathbf{pp}'}|^2 K(\mathbf{p}, \mathbf{p}') >> \times$$

$$\times \delta(eV - \Delta) , \qquad (2)$$

where $N(0)$ is the density of states at the Fermi level; n_f is the rare-earth ion concentration; N_k and N_i are the population numbers for the ground and excited CEF states; $W^{ik}_{\mathbf{pp}'}$ is the matrix element for the electron–CEF- level interaction for the rare-earth ion transition between an initial and a final state, and $K(\mathbf{p}, \mathbf{p}')$ is the point-contact weight factor. Therefore, $g_f(eV)$ depends on temperature and voltage. At zero temperature one has $N_i = (eV - \Delta)\Theta(eV - \Delta)/2(eV + \Delta)$ and $N_k = 1 - N_i$. The background in Eq. (1) has a contribution with *negative* sign. It reflects the diminution of probability of the inelastic electron scattering by the CEF levels at $eV > \Delta$, because the level population changes with voltage.

In addition to the CEF-level scattering processes, the electron-phonon interaction must be taken into account [13],

$$-\frac{d^2I}{dV^2}(eV) \sim g_{\text{ph}}(eV) +$$

$$+\left[\frac{\gamma}{2}\frac{eV}{eV + \hbar\omega_0} g_{\text{ph}}(eV) + \gamma \int_0^{eV} \frac{g_{\text{ph}}(\varepsilon)}{\varepsilon + \hbar\omega_0} d\varepsilon\right], \quad (3)$$

where $g_{\text{ph}}(eV)$ is electron-phonon spectral function, $\gamma = 0.58$, and ω_0 is the phonon escape frequency, $\omega_0 = \omega_D(l_{\text{ph}}\, l_r)/d^2$, determined by the relation between the inelastic l_{ph} and elastic l_r phonon path lengths and the contact diameter d; and ω_D is the Debye phonon frequency. In contrast to $g_f(eV)$, the spectral function $g_{\text{ph}}(eV)$ is temperature and voltage independent. The two last terms in Eq. (3) correspond to the background signal caused by the stimulated phonon emission and reabsorption of nonequilibrium phonons by conduction electrons.

The PC response to high-frequency irradiation depends on the relation between the external field frequency ν and the inverse relaxation times τ_i of the intrinsic electron scattering processes, which are responsible for the nonlinearity of the I-V curve. Frequency dispersion of the response occurs when $2\pi\nu\tau_i \sim 1$. For instance, the electron-phonon or electron–CEF-level relaxation are very fast processes, with characteristic frequencies $\nu_{e\text{–ph}}$, $\nu_{e\text{–}f} \sim 10^{13}$ Hz. The reabsorption of nonequilibrium phonons having the Debye energy by conduction electrons takes place more slowly, with $\nu_{\text{ph}\text{–}e} \sim 10^9$–$10^{10}$ Hz [10]. The CEF-level relaxation on electrons, as was estimated in [12], has a frequency $\nu_{f\text{–}e} \sim \nu_{e\text{–}f}\, n\Delta/n_f\, \varepsilon_F \sim 10^{11}$ Hz (n_f is the concentration of rare-earth atoms, and ε_F is the Fermi energy). For irradiation frequencies $\nu >> \nu_{f\text{–}e}$, $\nu_{\text{ph}\text{–}e}$ the background signal in the PC spectrum (Eqs. (1),(2)) drops like $[1 + (\nu/\nu_i)^2]^{-1}$ with increasing frequency [12,13] (ν_i denotes the CEF level-electron or phonon-electron collision frequency).

In this paper we report the experiments combining the low-frequency PC spectroscopy of $PrNi_5$-Cu contacts with measurements of the response to microwave and FIR irradiation up to 525 GHz for the same contacts. These frequencies are comparable with $\nu_{f\text{–}e}$ but are not large enough to cause considerable smearing the features of the CEF levels on the I-V curve by transition to the quantum regime of radiation detection [14,15]. Small broadening of the spectral lines takes place only for the highest frequency we have used and was taken into account as follows below.

Experiment

The PCs were formed between copper tip and the polished surface of the $PrNi_5$ single crystal with the contact axis parallel to the C axis. The choice of the «needle-plane» configuration was aimed at obtaining the best electrodynamic coupling of the contact with the high-frequency field. The contacts were produced in liquid helium by bringing two electrodes together with a precise differential screw mechanism. The contact resistances ranged from a few ohms to about twenty ohms. All measurements were done at temperature 1.5–1.7 K in superfluid helium to avoid the bubble boiling causing unstabilities of the rf power in the contact area. The electromagnetic radiation was generated by reflex klystron oscillators in the microwave range. A methyl alcohol submillimeter-wavelengths laser,

optically pumped by a cw carbon dioxide laser, was used as a source of FIR radiation. The radiation was delivered to the PC by a standard x-band waveguide with a smooth transition to a 2×23 mm cross section [9,16], or through a lightpipe with a focusing cone [17]. For monitoring the power level a small part of the radiation was reflected to a semiconductor detector by a beam splitter.

In a measuring cycle both the second-harmonic amplitude of the low-frequency (1.873 kHz) modulating current and the response signal — the difference of the I-V curve under and without rf irradiation (chopped by 2.433 kHz), were registered versus the bias voltage using a conventional lock-in technique for the same contact. In the small-signal limit ($V(t) = V_0 + v_1 \cos(2\pi\nu t)$, $v_1 << V_0$) both these quantities are proportional to the second derivative of the I-V curve $d^2V/dI^2 = -(d^2I/dV^2) \times (dV/dI)^3$ [14,16]. To avoid the modulation broadening of the PC spectra the intensity of rf irradiation and low frequency ac current were adjusted to the minimal levels providing an output signal amplitude about 1 μV.

Results and discussion

The experimental data obtained for the $PrNi_5$-Cu contacts are plotted in Fig. 1. Both the low-frequency and high-frequency PC spectra show the spectral features* that have been well established in previous studies [4,5] for these materials. The pronounced sharp peak at $eV \sim 4.2$ meV is connected with the Pr^{3+} ion transitions ($\Gamma_4 \to \Gamma_{5,A}$) from the ground state Γ_4. Additional singularities at 13 and 30 meV, corresponing to the CEF excitations ($\Gamma_4 \to \Gamma_3$) and ($\Gamma_4 \to \Gamma_{5B}$), are rather week. The peak at 9 meV and the wide maximum at 17 meV are usually ascribed to the characteristic phonon frequencies in $PrNi_5$ and Cu [4,5].

Unfortunately, in contrast to low-frequency measurements, the high-frequency current amplitude in point contacts is unknown. Therefore, in order to make a comparison between the spectral line heights in different frequency ranges the high-frequency data were multiplied by scaling factors. All the measurements were done in the small-signal limit, where the spectral line amplitudes were proportional to the power level of the high-frequency field and therefore the scaling procedure did not modify the shape of singularities. The normalization was carried out in an energy range where the external field frequency is much smaller than the

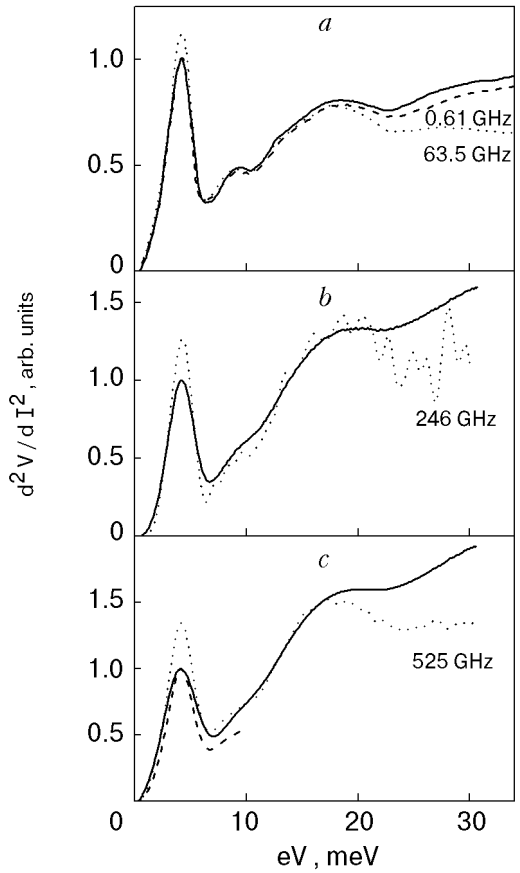

Fig. 1. Point-contact spectra (solid lines) and response signals at different frequencies (dashed and dotted lines). The dashed line in (c) — response signal fitted to audio-frequency data at $V = 4.2$ meV. The contact resistances are: $R_0 = 2.8\Omega$ for (a) and $R_0 = 7.4\Omega$ for (b, c).

intrinsic characteristic frequency of the scattering events determining the PC spectral singularities. For instance, the external frequency $\nu_1 = 0.61$ GHz for the PC spectrum in Fig. 1,a is much smaller than the characteristic frequencies of electron–CEF-level and CEF-level–electron relaxation processes ($\nu_1 << \nu_{e-f}, \nu_{f-e}$) which are responsible for the main peak at $eV = 4.2$ meV. The data at $\nu_1 = 0.61$ GHz were therefore fitted to the low-frequency peak at that energy. The frequency ν_1 is approximately equal to the thermal relaxation frequency, estimated as 0.5 GHz (see also [11,18]). The difference between these curves in Fig. 1,a increases slightly with energy but is quite small, showing the weak influence of heating effects in the contact. At $eV = 4.2$ meV the heating is negligible, so the normalization we have used is correct. The other rf spectra for $\nu_2 = 63.5$, $\nu_3 = 246$, and

* We neglected the small negative thermoelectric contribution (~ 5%) to the signal at $V \to 0$.

$\nu_4 = 525$ GHz were normalized to the audio-frequency data in the energy range 7–17 meV, where the contact resistance is mainly determined by an electron–phonon scattering processes (ν_2 , ν_3 , $\nu_4 << \nu_{e-ph}$). The phonon reabsorption background still has a rather low level in this energy interval. The large noise on the $\nu_3 = 246$ GHz curve is due to the smaller signal amplitude, because the laser power is about ten times smaller for this frequency compared to ν_4 . Therefore a larger value of the scaling factor has to be used for the fitting of the ν_3 data to audio-frequency spectrum.

It should be remarked that there is an additional problem in comparing the low-frequency PC spectra with the FIR data. The photon energy of $\nu_3 = 246$ GHz radiation ($h\nu_3 = 1$ meV) is equal to the amplitude of the low-frequency modulation ($ev_1 = = 1$ meV) and these two spectra can be directly compared (Fig. 1,*b*). But for $\nu_4 = 525$ GHz the photon energy ($h\nu_4 = 2.2$ meV) is larger than ev_1 and is comparable with the CEF linewidth at 4.2 meV. Therefore, the spectral line is smeared in energy range $eV = h\nu_4$ because the quantum regime of radiation detection [14,15] occurs for this frequency even in the low-power limit used in our experiments. That is why the low-frequency spectra in Fig. 1,*c* were calculated by standard smearing procedure [6] with $ev_1 = 2.2$ meV for the curve in Fig. 1,*b* (experiments at ν_3 and ν_4 were performed with the same contact) to permit a correct comparison of the low-frequency and FIR data. Thus, each set of curves in Fig. 1 are characterized by an equal instrumental broadening.

For additional confirmation of the scaling procedure we have used the CEF peak for $\nu_4 = 525$ GHz, normalized to the audio-frequency data at $eV = 4.2$ meV and shown by the dashed curve in Fig. 1,*c*. In that case the CEF linewidth turns out to be abnormally narrow, confirming the validity of the fitting procedure previously described.

The difference between the audio- and high-frequency spectra in Fig. 1 appears in the CEF peak position (4.2 meV) and in the high-energy range. It is well known [7,8,13] that the background signal in the PC spectra at high energy $eV \geq \hbar\omega_D$ is determined by the phonon-electron reabsorption processes. At high frequencies $\nu > \nu_{ph-e}$ the number of nonequilibrium phonons does not follow the high-frequency voltage induced in the contact. The higher the frequency, the smaller the fraction of these phonons that relaxes to the equilibrium state synchronously with the voltage, thus *decreasing* the contribution to the second-derivative signal. The background frequency dispersion has been studied in detail [9,19] and the characteristic relaxation frequencies ν_{ph-e} have been determined for several simple metals. Our data in Fig. 1 are in good agreement with that previous measurements.

The characteristic frequency of phonon-electron scattering ν_{ph-e} for the compound $PrNi_5$ is estimated as about 3–5 GHz, and therefore the condition $\nu >> \nu_{ph-e}$ is fulfilled for the three frequencies ν_2 , ν_3 , ν_4 in our experiments, and the phonon background damping has to be independent of frequency for these spectra. Indeed, as is shown in Fig. 1,*b,c*, the rf background is decreased to an identical value for the same contact. A slightly different background is observed in Fig. 1,*a* for another contact because of the different conditions of phonon escape (the larger diameter, different concentration of crystal lattice defects, etc.). But different phonon transport conditions do not create an obstacle for the correct comparison of the CEF-peak amplitude because the *f*-shell excitation rate are dependent on transport of conduction electrons and these excitations are localized on the $PrNi_5$ ions.

In the low-energy region the high-frequency signal *increases*, showing growth of the CEF-peak amplitude, opposite to the behavior in the high-energy region (Fig. 1). In accordance with Eq.(1) the background part of the PC spectrum for CEF-level excitations has a *negative* contribution, in contrast to the phonon part of spectrum (Eq. (3)). At high frequencies $\nu > \nu_{f-e}$ the population numbers N do not follow the high-frequency voltage, the background part of the PC spectrum decreases, similarly to the phonon reabsorption processes discussed above, and the high-frequency second-harmonic amplitude becomes exactly equal to $g_f(eV)$, as was shown in the theory [12]. In our experiments the difference between the I-V curves under and without irradiation has been determined. In such a method the steady-state population of excited f levels is increased under high-frequency irradiation (similarly to the bolometric effect in the phonon reabsorption study [9]), increasing the probability of reverse transition to the ground state. This brings about an additional contribution to measured signal (renormalizing term $\frac{1}{2}\, g_f(eV)$ in Eq. (1)) and the output signal amplitude becomes equal to $1.5\, g_f(eV)$ (see Eq. (34) in Ref.12).

For qualitative analysis we calculated the negative background components of the CEF spectrum from Eq. (1). The spectral line $g_f(eV)$ was represented by a Lorentzian curve with a small exponential part in the low-energy range and a linewidth equal to the experimental peak width for

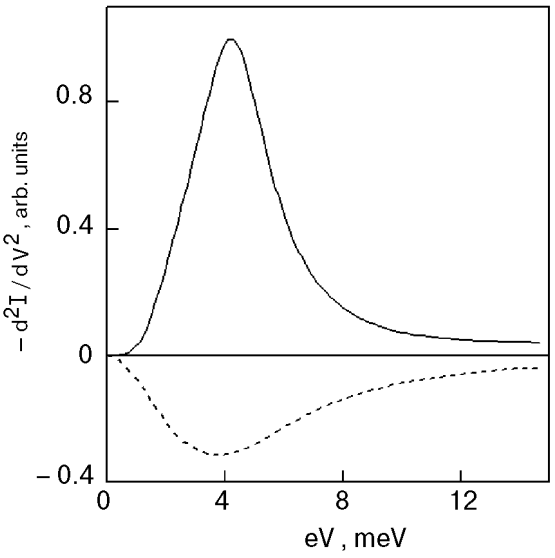

Fig. 2. Components of PC spectrum for CEF-level excitations: spectral part $g_f(eV)$ (solid line), negative background signal (dashed line).

$\nu_4 = 525$ GHz. The result is shown in Fig. 2 by the dashed line.

The frequency dispersion of the absolute value of the negative background signal for the CEF-level-electron scattering processes is shown in Fig. 3, where $B_\nu = (S_\infty - S_\nu)/(S_\infty - S_0)$; S_0 is the CEF-peak heihgt at audio frequency, and S_ν is the height at high frequency ν. The experimental data are represented as three sets of points for three different values of S_∞ : $S_\infty = S(\nu_4 = 525\text{GHz})$ (solid circles), $S_\infty = 1.1S(\nu_4)$ (squares), and $S_\infty = 1.3S(\nu_4)$ (diamonds). Two later series are shown for the case when the signal saturation was not reached in our experiments, i.e., $2\pi\nu_4\tau_{f-e} < 1$. The three curves in

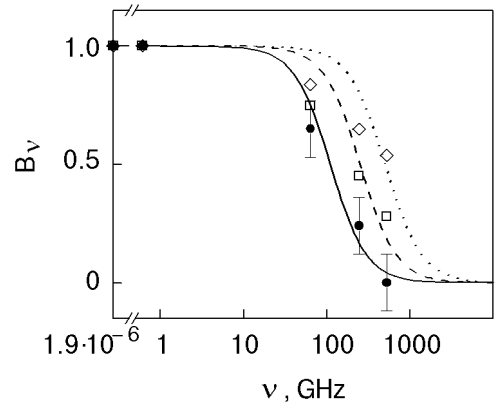

Fig. 3. Frequency dispersion of background signal. The sets of points were obtained from the experimental data normalized by different S_∞ equal to: $S_\infty = S(\nu_4 = 525$ GHz) (solid circles), $S_\infty = 1.1S(\nu_4)$ (squares) and $S_\infty = 1.3S(\nu_4)$ (diamonds). The lines represent the background amplitude calculated for different ν_{f-e} values: 110 GHz (solid), 250 GHz (dashed), and 500 GHz (dotted line).

Fig. 3 show plots of $[1 + (\nu/\nu_i)^2]^{-1}$ for three values of the characteristic frequencies ν_{f-e} : 110 GHz (solid), 250 GHz (dashed), and 500 GHz (dotted line). The best coincidence between the experimental points and the calculated curves occurs in the range 110–250 GHz. Thus we can evaluate the CEF-level – electron relaxation frequency ν_{f-e} as ~ 200 GHz.

It should be emphasized that the results in Fig. 3 are essentially dependent on the fitting procedure in Fig. 1. But, as was mentioned above, the phonon background damping is independent of frequency at $\nu >> \nu_{ph-e}$, and any deviations in the scaling procedure have to be the same for all S_ν values. These deviations do not significantly influence the estimation of ν_{f-e} because the ratio of measured signals is used in calculations. Thus, for instance, if the differences between the rf and audio-frequency spectra were decreased by two or three times, the B_ν values would coincide with the points shown in Fig. 3.

It should be noted that in our experiments the absolute value of the background signal B is about $0.4g_f$ (Fig. 1,*c*) at the CEF-peak position, but the calculated B~ 0.3 in Fig. 2. This distinction is possibly caused by the large renormalizing coefficient $^1/_2$ connected with reverse CEF-level transitions, which was considered in the theory [12], where a strong localization of *f*-shell excitations on Pr^{3+} ions was assumed. Moreover, the ion-ion and *f*-level–phonon interaction were neglected. This results in a very narrow spectral line in the PC spectrum (δ-function shape at $T = 0$ which is smeared to 0.74 meV at 1.6 K). In special experiments the halfwidth of the CEF peak at $eV = 4.2$ meV has been measured for different audio-frequency current modulation amplitudes. Extrapolating this data to $v_1 \to 0$, we estimated the linewidth as ~ 1.93 meV at $T = 1.6$ K. This means that additional dissipation mechanisms should be taken into account compared to [12]. There are various possible causes of the CEF-line broadening: bilinear and quadrupolar exchange interaction between rare-earth ions, a quadrupolar contribution to the spin-disorder resistivity, and *f*-shell-excitation–phonon coupling, as have been well established for $PrNi_5$ crystals by magnetoelastic, resistivity and neutron diffraction experiments [1,2,20]. These interactions destroy the strong localization of *f*-shell excitations and therefore result in a decreasing of the second term amplitude in Eq. (1). Moreover, the inelastic neutron scattering study [21] shows the drop and disappearance of the *f*-spectral line in the energy range ~ 4.2 meV during the crystal-to-amorphous-state

transition. Hence, some crystal lattice irregularities at contact forming assist the further broadening of the f-shell–excitation line in the PC spectrum. We believe that in the general case all these phenomena are responsible for the discrepancies between our experimental data and the theory [12].

Conclusion

The PC spectra measurements over a wide frequency range give an excellent opportunity to distinguish between the different electron scattering mechanisms causing the nonlinear contact conductivity when the electromagnetic field frequency satisfies the condition $2\pi\nu\tau_i \sim 1$. Similar experiments allow one to study the kinetics of relaxation phenomena in metals. In this paper we have demonstrated the applicability of this method to the investigation of $PrNi_5$-Cu point contacts. It was found that the rf response signal amplitude *decreases* for thermal and phonon reabsorption processes while it *increases* for the CEF-level relaxation in the limit $2\pi\nu\tau_{f-e} > 1$. The CEF-level relaxation was studied in detail, and a characteristic frequency $\nu_{f-e} \sim 200$ GHz was estimated. It should be noted that the experimental data show the presence of f-level excitation damping, which smears the corresponding peak in the PC spectrum.

Acknowlegments

We would like to thank A.N. Omelyanchouk for helpful discussions. Part of this work was supported by International Science Foundation Grant No. U9V000.

1. V.M.T.S. Barthem, D. Gignoux, A. Naït-Saada, and D. Schmitt, *Phys. Rev.* **B37**, 1733 (1988).
2. J.A. Blanco, M. Reiffers, D. Gignoux, D. Schmitt, and A.G.M. Jansen, *Phys. Rev.* **B44**, 9325 (1991).
3. P.A. Alekseev, A. Andreeff, H. Griesmann, L.P. Kaun, B. Lipplod, W. Matz, I.P. Sadikov, O.D. Christyakov, I.A. Markova, and E.M. Savitskii, *Phys. Status Solidi (b)* **97**, 87 (1980).
4. A.I. Akimenko, N.M. Ponomarenko, I.K. Yanson, S. Janos, and M. Reiffers, *Fiz. Tverd. Tela* **26**, 2264 (1984) [*Sov. Phys. Solid State* **26**, 1374 (1984)].
5. M. Reiffers, Yu.G. Naidyuk, A.G.M. Jansen, P. Wyder, I.K.Yanson, D. Gignoux, and D. Schmitt, *Phys. Rev. Lett.* **62**, 1560 (1989).
6. A.V. Khotkevich and I.K. Yanson, *Atlas of Point Contact Spectra of Electron-Phonon Interaction in Metals*, Kluwer Academic Publishers, Boston (1995).
7. A.G.M. Jansen, A.P. van Gelder, and P. Wyder, *J. Phys.* **C13**, 6073 (1980).
8. I.K. Yanson and O.I. Shklyarevskii, *Fiz. Nizk. Temp.* **12**, 899 (1986) [*Sov. J. Low Temp. Phys.* **12**, 509 (1986)].
9. O.P. Balkashin, I.K. Yanson, and Yu.A. Pilipenko, *Fiz. Nizk. Temp.* **13**, 389 (1987) [*Sov. J. Low Temp. Phys.* **13**, 222 (1987)].
10. O.P. Balkashin, *Fiz. Nizk. Temp.* **18**, 659 (1992) [*Sov. J. Low Temp. Phys.* **18**, 470 (1992)].
11. O.P. Balkashin and I.I. Kulik, *Physica* **B218**, 50 (1996).
12. I.O. Kulik, A.M. Omelyanchouk, and I.G. Tuluzov, *Fiz. Nizk. Temp.* **14**, 149 (1988) [Sov. J. Low Temp. Phys. 14, 89 (1988)].
13. I.O. Kulik, *Fiz. Nizk. Temp.* **11**, 937 (1985) [*Sov. J. Low Temp. Phys.* **11**, 516 (1985)].
14. J. R. Tucker, *IEEE J. Quantum Electron.* **15**, 1234 (1979).
15. A. I. Omelyanchouk and I. G. Tuluzov, *Fiz. Nizk. Temp.* **9**, 284 (1983) [*Sov. J. Low Temp. Phys.* **9**, 142 (1983)].
16. O. P. Balkashin, R.J.P. Keijsers, H.van Kempen, Yu.A. Kolesnichenko, and O.I. Shklyarevskii, *Phys.Rev.* **B58**, 1294 (1998).
17. R.V. van der Heijden, Ph.D.Thesis, *University of Nijmegen* (1982).
18. O.P. Balkashin, I.K. Yanson, V.S. Solov'ev, and A.Yu. Krasnogorov, *Zh. Tekh. Phys.* **52**, 811 (1982) [*Sov. Tech. Phys. 27*, 522 (1982)].
19. O.P. Balkashin, I.K. Yanson, and Yu.A. Pilipenko, *Fiz. Nizk. Temp.* **17**, 221 (1991) [*Sov. J. Low Temp. Phys.* **17**, 114 (1991)].
20. V.L. Aksenov, E.A. Goremychkin, E. Muhle, Th. Frauenheim, and W. Buhrer, *Physica* **B120**, 310 (1983).
21. P.A. Alekseev, V.N. Lazukov, V.G. Orlov, I.P. Sadikov, and J.B. Suck, *Physica* **B180–181**, 167 (1992).